Dynamics of Spin-Stabilized Satellites during Extension of Long Flexible Booms

D. B. CHERCHAS*
Institute for Aerospace Studies, University of Toronto Toronto, Canada

Nomenclature

b	= perpendicular distance of boom root from $\mathbf{i}_3$
$E_2(\xi), E_3(\xi)$	= nondimensional mode shapes for boom vibration in $\mathbf{j}_2$, $\mathbf{j}_3$ directions, respectively
EI	= flexural stiffness of boom
h	= perpendicular distance of boom root above $\mathbf{i}_1$, $\mathbf{i}_2$ plane
$\mathbf{i}_1,\mathbf{i}_2,\mathbf{i}_3$	= principal axes of main body, $\mathbf{i}_3$ is nominal spin axis
$\mathbf{j}_1,\mathbf{j}_2,\mathbf{j}_3$	= boom base set of axes, $\mathbf{j}_1$ is nominal boom line
I	= inertia tensor of main body
I_{11},I_{22},I_{33}	= principal moments of inertia of main body along $\mathbf{i}_1$, $\mathbf{i}_2$, $\mathbf{i}_3$, respectively
$l(t)$	= length of boom
M_b, M_t	= boom and tip total masses
M_m	= mass of main body
M_{st}	= total satellite mass
s	= distance along boom center line from boom root to point on boom
$\mathbf{x}$	= position of mass element of boom as seen in $\mathbf{j}_1$, $\mathbf{j}_2$, $\mathbf{j}_3$ set
$\alpha_3,\alpha_2,\alpha_1$	= Euler angles (3,2,1 sequence) relating $\mathbf{i}_1$, $\mathbf{i}_2$, $\mathbf{i}_3$ to inertial attitude axes at main body mass center. Axis 3 of both sets parallel in nominal spin
$\dot{\alpha}_{3D}$	= change in spin rate
$\Phi_2(t),\Phi_3(t)$	= modal amplifiers i.e., $x_2 = \Phi_2 lE_2$, $x_3 = \Phi_3 lE_3$
Ψ	= angle between $\mathbf{j}_1$ and $\mathbf{i}_1$ measured on projection of $\mathbf{j}_1$ in $\mathbf{i}_1 - \mathbf{i}_2$ plane
ρ	= mass per unit length of boom
ω	= angular velocity of main body

Introduction

SATELLITES employing long flexible booms for ionio-spheric sounding or telemetering purposes typically have these long appendages compactly stored until the satellite is in its approximate operational posture in orbit. During deployment, the flexible appendages will cause the main body to despin and change its nutation—precession characteristics. Moreover, the booms will be subjected to bending moments due to environmental inputs and the inertial loading from the main body motion. The purpose of this study is to determine the maximum nutation-precession angles expected to remain after deployment and to find the maximum bending moments and deflections the booms will experience.

This analysis neglects environmental inputs during deployment and considers a configuration in which all booms are nominally perpendicular to the nominal spin axis with the projection of their nominal line passing through the nominal spin axis (see Fig. 1).

Josloff[1] has found expressions for maximum bending moments on deploying booms for a 'point mass' main body and total angular momentum vector assumed to lie along a principal axis; Lang and Honeycutt[2] have found design methods for critical values of boom bending moments during deployment by considering the boom masses to be located at appropriate radii of gyration; Bowers and Williams[3] have studied boom deployment timing to ensure gravity-gradient capture; Cloutier[4] has simplified the study of boom deployment of heavy tip masses by neglecting boom mass. A more rigorous analysis is presented.

Received January 11, 1971; revision received March 17, 1971. This work was carried out under an AERCOL contract to Spar Aerospace Products Ltd., Toronto, Canada and the Defense Research Board of Canada (DIR Project E126). The author gratefully acknowledges the helpful comments and suggestions given by P. C. Hughes and N. K. Phung.

* Graduate Student.

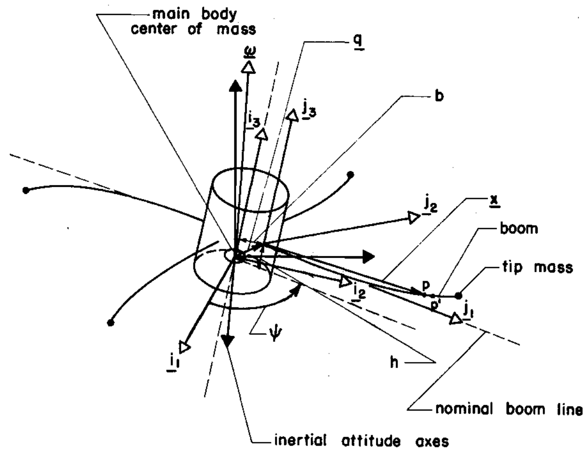

Fig. 1 General satellite configuration.

Equations of Motion

The equations of motion of a configuration (elastic degrees of freedom are discretized by modal analysis) typified in Fig. 1 are developed from Lagrange's equations

$$d/dt(\partial T/\partial \dot{q}_j) - \partial T/\partial q_j + \partial U/\partial q_j = 0 \tag{1}$$

in which T is the configuration kinetic energy about the total mass center

$$T = \tfrac{1}{2}\boldsymbol{\omega}^T I\boldsymbol{\omega} + \tfrac{1}{2}M_m\dot{\mathbf{r}}\cdot\dot{\mathbf{r}} + \sum_i \tfrac{1}{2}\int (\dot{\mathbf{r}} + \dot{\mathbf{q}}_i + \dot{\mathbf{x}}_i)\cdot (\dot{\mathbf{r}} + \dot{\mathbf{q}}_i + \dot{\mathbf{x}}_i)dm \tag{2}$$

where

$$\mathbf{r} = -\sum_i \int [(\mathbf{q}_i + \mathbf{x}_i)/M_{st}]dm$$

Note that the integrals are over the entire boom mass including unextended boom and tip mass. Moreover, U is the boom strain energy

$$U = \sum_i \frac{1}{2} EI_i \int_0^l \kappa_i^2 ds_i \tag{3}$$

where

$$\kappa^2 = \sum_{i=1}^{3}\left(\frac{\partial^2 x_i}{\partial s^2}\right)^2$$

$$ds = [1 + (dx_2/dx_1)^2 + (dx_3/dx_1)^2]^{1/2}dx_1$$

The equations for torque-free motion are developed from Eq. (1) by using as generalized coordinates $\alpha_1,\alpha_2,\alpha_3,\Phi_{2i}$ and Φ_{3i}, where α_1,α_2, and α_3 describe the main body motion and Φ_{2i}, Φ_{3i} the boom vibrations.

The modes of vibration are found from the following considerations. We consider a thin rod mounted as a cantilever onto the satellite body as shown in Fig. 1. The differential equation of boom shape is

$$\frac{d}{ds}\left(\frac{d\mathbf{x}}{ds}\right) = \frac{\boldsymbol{\tau}\times(d\mathbf{x}/ds)}{EI} \tag{4}$$

where

$$\boldsymbol{\tau} = -\int_s^l \rho[\{\mathbf{x}(s')-\mathbf{x}(s)\}\times\mathbf{a}]ds' \tag{5}$$

$$\mathbf{a} = (\dot{\omega}) \times \mathbf{R} + 2\omega \times (\dot{\mathbf{R}}) + \omega \times (\omega \times R) + (\ddot{\mathbf{R}}), \qquad \mathbf{R} = \mathbf{q} + \mathbf{x} \tag{6}$$

Inserting Eqs. (5) and (6) into Eq. (4), assuming that $dx_1/ds \cong 1$, $dx_2/ds \cong dx_2/dx_1$, $dx_3/ds \cong dx_3/dx_1$, $\Sigma_i(M_{bi} + M_{ti})/M_m \ll 1$, as well that ω_1, $\omega_2,\dot{\omega}_1,\dot{\omega}_2,\dot{\omega}_3$, $x_2',x_3',\dot{x}_2',\dot{x}_3'$ are sufficiently small that terms of order two and higher in these quantities can be ignored, we obtain, with $\Psi = 0$,

$$EI\frac{\partial^2 x_2(x_1,t)}{\partial x_1^2} = -\int_{x_1}^{l} \rho\,\{[\dot{\omega}_3(b + x_1') - \dot{\omega}_1 h + 2\omega_3 \dot{l} + \omega_2\omega_3 h - \omega_3^2 x_2(x_1',t) + \ddot{x}_2(x_1',t)](x_1' - x_1) + [-\omega_3^2(b + x_1') + \ddot{l}][x_2(x_1',t) - x_2(x_1,t)]\}dx_1' \tag{7}$$

$$EI\frac{\partial^2 x_3}{\partial x_1^2}(x_1,t) = -\int_{x_1}^{l} \rho\{[-\dot{\omega}_2(b + x_1') - 2\omega_2 \dot{l} + \omega_1\omega_3(b + x_1') + \ddot{x}_3(x_1',t)](x_1' - x_1) + [-\omega_3^2(b + x_1') + \ddot{l}][x_3(x_1',t) - x_3(x_1,t)]\}dx_1' \tag{8}$$

where prime (′) denotes values at P' (see Fig. 1). Equations (7) and (8) are subject to boundary conditions to be shown shortly. Introducing the notation

$$x_1' = l\xi', \quad x_2(x_1',t) = l\eta(\xi',\phi), \quad x_3(x_1',t) = l\zeta(\xi',\phi),$$
$$\phi = \omega_3 t, \quad \epsilon = b/l,$$
$$N_1 = (-\dot{\omega}_1 h + \omega_2\omega_3 h)/l\omega_3^2, \quad N_2 = (\omega_1\omega_3 - \dot{\omega}_2)/\omega_3^2,$$
$$\lambda = \rho l^4\omega_3^2/EI, \quad \lambda' = M_t l^3\omega_3^2/EI, \quad r = \lambda'/\lambda$$

Eqs. (7) and (8) can be written in nondimensional form. Integral Eqs. (7) and (8) can be reduced to fourth-order partial differential equations.[5] Regarding l and ω_3 as constant, the equations for the boom vibration and the associated boundary conditions can be shown to have the form

$$\eta_{\xi\xi\xi\xi} - \frac{\lambda}{2}[1 - \xi^2 - 2\epsilon\xi + 2\epsilon + 2r(1 + \epsilon)]\eta_{\xi\xi} + \lambda[\epsilon + \xi]\eta_\xi - \lambda\eta + \lambda\eta_{\phi\phi} = -\lambda N_1(\phi),$$
$$\eta(0,\phi) = 0, \quad \eta_\xi(0,\phi) = 0, \quad \eta_{\xi\xi}(1,\phi) = 0, \tag{9}$$
$$\eta_{\xi\xi\xi}(1,\phi) = \lambda'[\eta_{\phi\phi}(1,\phi) - \eta(1,\phi) + \eta_\xi(1,\phi)(1 + \epsilon) + N_1(\phi)]$$

$$\zeta_{\xi\xi\xi\xi} - \frac{\lambda}{2}[1 - \xi^2 - 2\epsilon\xi + 2\epsilon + 2r(1 + \epsilon)]\zeta_{\xi\xi} + \lambda[\epsilon + \xi]\zeta_\xi + \lambda\zeta_{\phi\phi} = -\lambda N_2(\phi)(\epsilon + \xi),$$
$$\zeta(0,\phi) = 0, \quad \zeta_\xi(0,\phi) = 0, \quad \zeta_{\xi\xi}(1,\phi) = 0, \tag{10}$$
$$\zeta_{\xi\xi\xi}(1,\phi) = \lambda'[\zeta_{\phi\phi}(1,\phi) + \zeta_\xi(1,\phi)(1 + \epsilon) + N_2(\phi)(1 + \epsilon)]$$

Thus, we have partial differential equations which are forced by the precession—nutation inputs N_1 and N_2, where N_1 and N_2 are close to being periodic (for symmetric rigid body, exactly periodic) with a frequency in ϕ of Ω_n. If we assume particular solutions of the form

$$\eta_p(\xi, \phi) = E_2(\xi)P(\phi), \quad \zeta_p(\xi, \phi) = E_3(\xi)P(\phi)$$

and use

$$N_1(\phi) = F_1P(\phi), \quad N_2(\phi) = F_2P(\phi)$$

where

$P_{\phi\phi} = -\Omega_n^2P$, $|P_{\max}| = 1$, then Eqs. (9) and (10) become

$$E_2'''' - \frac{\lambda}{2}[1 - \xi^2 - 2\epsilon\xi + 2\epsilon + 2r(1 + \epsilon)]E_2'' + \lambda[\epsilon + \xi]E_2' - \lambda(1 + \Omega_n^2)E_2 = -\lambda F_1, \tag{11}$$

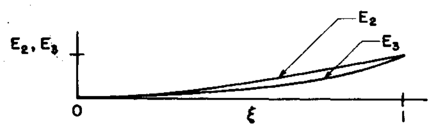

Fig. 2 Boom mode shapes.

$$E_2(0) = 0, \quad E_2'(0) = 0, \quad E_2''(1) = 0,$$
$$E_2'''(1) = \lambda'[-(\Omega_n^2 + 1)E_2(1) + E_2'(1)(1 + \epsilon) + F_1]$$

$$E_3'''' - \frac{\lambda}{2}[1 - \xi^2 - 2\epsilon\xi + 2\epsilon + 2r(1 + \epsilon)]E_3'' + \lambda[\epsilon + \xi]E_3' - \lambda\Omega_n^2E_3 = -\lambda F_2(\epsilon + \xi), \tag{12}$$
$$E_3(0) = 0, \quad E_3'(0) = 0, \quad E_3''(1) = 0,$$
$$E_3'''(1) = \lambda'[-\Omega_n^2E_3(1) + E_3'(1)(1 + \epsilon) + F_2(1 + \epsilon)]$$

where prime (′) denotes differentiation w.r.t. argument.

The solutions of the linear two point boundary value Eqs. (11), and (12), give suitable modes to identify realistic degrees of freedom of boom lateral vibration under nutation—precession inertial loading.

Solution

The configuration equations of motion, Eq. (1), are expressible as

$$A(t)\dot{\mathbf{Y}}(t) = B(t)\mathbf{Y}(t) + \mathbf{C}(t) \tag{13}$$

where $\mathbf{Y}(t)$ is defined by

$$\mathbf{Y}(t)^T = [\dot{\alpha}_1,\dot{\alpha}_2,\dot{\alpha}_{3D},\dot{\phi}_{2i}\ldots\dot{\phi}_{3i}\ldots,\alpha_1,\alpha_2,\alpha_{3D},\Phi_{2i}\ldots,\Phi_{3i}\ldots]$$

and matrices A, B, $\mathbf{C}$ are functions of time because l_i, $\dot{l}_i$, $\ddot{l}_i$ depend on time during the extension history. Premultiplying Eq. (13) by $A^{-1}(t)$ we obtain

$$\dot{\mathbf{Y}}(t) = A^{-1}(t)B(t)\mathbf{Y}(t) + A^{-1}(t)\mathbf{C}(t) \tag{14}$$

Equation (14) is integrated numerically throughout the extension. Equations (11) and (12) are used to obtain modes E_2, E_3 for the boom vibration degrees of freedom required in Eq. (1). The numerical solution of Eq. (14) is approximated by using constant E_2, E_3 through small $\Delta l/l$. E_2 and E_3 are updated with the latest ω_3, l and average Ω_n at the beginning of each $\Delta l/l$.

Table 1 Two boom satellite dynamics

Quantity		Value
Greatest α_1 magnitude, rad		0.0167
Greatest α_2 magnitude, rad		0.0197
Spin rate after boom extension, rad/sec		2.894
Typical $\alpha_{1\max}$ after boom extension, rad		0.0165
Typical $\alpha_{2\max}$ after boom extension, rad		0.0185
	Boom 1	Boom 2
Maximum bending moment magnitude in plane (from out of plane vibrations), lb-ft	0.0206 (23.5)[a]	0.0206 (23.5)[a]
Maximum bending moment magnitude normal to plane (from in plane vibration), lb-ft	0.0362 (22.61)	0.0357 (23.06)
Maximum total bending moment magnitude, lb-ft	0.0411 (22.61)	0.0408 (23.06)
Greatest tip deflection magnitude out of plane, ft	0.4214 (23.5)	0.4214 (23.5)
Greatest tip deflection magnitude in plane, ft	0.7851 (22.61)	0.7785 (23.06)
Greatest total tip deflection magnitude, ft	0.885 (22.61)	0.88 (23.06)

[a] Numbers in parentheses are boom lengths (ft) at which the maxima occur.

The detailed integration is monitored continually and maximum dimensionalized values of the desired variables in $\mathbf{Y}(t)$ are displayed.

The solutions of the boundary value problems, Eqs. (11) and (12), result in mode shapes in which greatest deflection and curvature appear at the boom tip and root, respectively, for all cases studied. Some typical shapes are shown in Fig. 2 for the example described later.

The integration of Eq. (14) clearly shows the main body motion being slightly (except for despin) altered by the effects of extension and vibration of the boom. Moreover, in cases where the instantaneous transient natural frequency of vibration of the booms is much higher than the nutation—precession frequency, the results show a high frequency transient vibration of the booms being modulated by the low frequency inertial loading they experience.

A number of cases were analyzed by the program. One such case was a single dipole boom pair being symmetrically extended from a main body with a nonsymmetric inertia ellipsoid. The parameters used are as follows: $I_{11} = 14.2$ slug-ft^2; $I_{22} = 13.78$ slug-ft^2; $I_{33} = 15.09$ slug-ft^2; $EI_i = 1.735$ lb-ft^2; $\rho_i = 1.685 \times 10^{-4}$ slug/ft; $M_{ti} = 4.115 \times 10^{-4}$ slug; $\dot{l}_i = 0.0417$ fps; $l_{i\text{final}} = 23.5$ ft; $b_i = 1.1$ ft; $h_i = 1.5$ ft; $\Psi_1 = 14°$; $\Psi_2 = 194°$

$$\text{Initial coning angle} \cong 1°$$

$$\dot{\alpha}_3(0) \cong 3.3 \text{ rad/sec}$$

The results appear in Table 1. A typical value for Ω_n, the nutation—precession frequency in ϕ, for this example varied between 0.075 and 0.1.

If Eqs. (7) and (8) are reduced to fourth-order partial differential equations without making the indicated simplifications in Eqs. (9) and (10), the general linearized partial differential equations of boom motion result. Another approach to the boom extension problem consists of solving these equations together with the equation for the conservation of the satellite angular momentum.

Several interesting effects are evident in the dynamics of a satellite with extending booms. For example, in-plane ($\mathbf{j}_2$) vibrations are influenced by despin and Coriolis forces as well as nutation. Out-of-plane ($\mathbf{j}_3$) vibrations are affected mainly by nutation. The "centrifugal stiffening" is greatest for out-of-plane vibrations. One result of such a combination of effects is that in-plane vibrations are nonsymmetric and can easily become greater than out-of-plane vibrations if the despin rate is high, as can be seen from Table 1.

Conclusions

The analysis and program developed are useful for determining the dynamics of satellites under deployment of long flexible booms and could be used to find the typical dynamics during normal operation after deployment. The program parameters are arbitrary within the confines of a spin-stabilized configuration and can be specified for each boom independently.

An example indicated that the satellite modelled should be left with a small "coning" angle after extension, and that its booms are not in danger of buckling. Increases in initial coning angle result in proportionate increases in maximum values. Thus, predictions for other initial coning angles can easily be made from Table 1 for the satellite modelled; this is to be expected, since the approximate equations of motion used are linear.

References

[1] Josloff, A. T., "Systems Constraints Imposed on Spacecraft Utilizing Long Extendible Rods with Attached Tip Masses," *AIAA/ASME 8th Structures, Structural Dynamics and Materials Conference*, AIAA, N. Y.

[2] Lang, W. E. and Honeycutt, G. N., "Simulation of Deployment Dynamics of Spinning Spacecraft," TN D-4074, Aug. 1967, NASA.

[3] Bowers, E. J. and Williams, C. E., "Optimization of RAE Satellite Boom Deployment Timing," *Journal of Spacecraft and Rockets*, Vol. 7, No. 9, Sept. 1970, pp. 1057–1062.

[4] Cloutier, G. J., "Dynamics of Deployment of Extendible Booms from Spinning Space Vehicles," *Journal of Spacecraft and Rockets*, Vol. 5, No. 5, May 1968, pp. 547–552.

[5] Hughes, P. C. and Cherchas, D. B., "Influence of Solar Radiation on the Spin Behaviour of a Satellite with Long Flexible Antennae," *CASI Transactions*, Vol. 2, No. 2, Sept. 1969, pp. 53–57.

Effects of Surface Roughness on Heat Transfer to Ablating Bodies

JIN H. CHIN*
Lockheed Missiles & Space Company, Sunnyvale, Calif.

Nomenclature

C_c = $(\rho_*/\rho_e)^{0.8}(\mu_*/\mu_e)^{0.2}$
k = roughness dimension
K_r = roughness correction factor
N = surface inward normal
R = roughness function
Re_k = roughness Reynolds Number $\rho_e u_e k/\mu_e$
Re_θ = momentum-thickness Reynolds Number $\rho_e u_e \theta/\mu_e$
St = zero-blowing Stanton Number
$\bar{St}$ = blowing Stanton Number
T = absolute Temperature
u = tangential velocity
μ = viscosity
ρ = density

Subscripts

c = between minimum and maximum values
e = at boundary layer edge
L = laminar boundary layer
T = turbulent boundary layer
r = rough surface
w = at wall conditions
$*$ = reference enthalpy conditions

Introduction

To include the effects of surface roughness on thermal response predictions for ablating bodies, an adequate theory must be able to account for the following: 1) effects of surface roughness on heating and pressure distribution, and 2) characterization of roughness variation with time during the heating environment history. The effects of surface roughness on turbulent skin friction and heat transfer have been studies by a number of investigators.[1-4] Some results indicate that large surface roughness increases the stagnation-point heat transfer.[5,6] Other results show that roughness does not increase the heat transfer at the stagnation point nor at other parts of the body when the flow remains laminar.[7] For nonblowing, smooth walls the method of Persh[8] provides a reasonable correlation with experimental heating data in the transitional boundary layer regime.[9] The formation of cross-hatching generally requires a supersonic transitional or turbulent boundary layer.[10] Large variation in heating exposure time required for initiation of cross-hatching for different

Received July 13, 1970; revision received February 22, 1971. The work was performed with support from Contract F0-4701-68-C-0299.

* Staff Engineer, Aero-Thermodynamics Department, Engineering Technology. Member AIAA.